AI Driven Autonomous Adaptative Feedback Welding Machine

Benedikt von Querfurth
FhG-ILT: Fraunhofer-Institut fur Lasertechnik ILT https://orcid.org/0009-0001-0384-7923
Shems-Eddine Belhout
sbelhout@epri.com
EPRI: Electric Power Research Institute https://orcid.org/0009-0004-8984-1902
Christian Knaak
FhG-ILT: Fraunhofer-Institut fur Lasertechnik ILT
Stefan Mann
FhG-ILT: Fraunhofer-Institut fur Lasertechnik ILT
Peter Abels
FhG-ILT: Fraunhofer-Institut fur Lasertechnik ILT
Carlo Holly
RWTH Aachen University TOS – Chair for Technology of Optical Systems
Jonathan Tatman
EPRI: Electric Power Research Institute
Darren Barborak
EPRI: Electric Power Research Institute
Mitch Hargadine
EPRI: Electric Power Research Institute

Research Article

Keywords:

Posted Date: November 2nd, 2024

DOI: https://doi.org/10.21203/rs.3.rs-4999627/v1

AI Driven Autonomous Adaptative Feedback Welding Machine

Benedikt von Querfurth[1], *Shems-Eddine* Belhout[3], *Christian* Knaak[1], *Stefan* Mann[1*], *Peter* Abels[1], *Carlo* Holly[1,2], *Jonathan* Tatman[3*], *Darren* Barborak[3], and *Mitch* Hargadine[3]

[1]Fraunhofer Institute for Laser Technology (ILT), 52074 Aachen, Germany

[2]RWTH Aachen University TOS – Chair for Technology of Optical Systems, 52074 Aachen, Germany

[3]Electric Power Research Institute (EPRI), 28262 NC Charlotte, United States

Abstract. The Gas Tungsten Arc Welding (GTAW) is a primary method for nuclear component fabrication and repair. Recent advancements in monitoring and automation technologies have made the shift toward fully automated arc welding more feasible, reducing the necessity for continuous human oversight. Two artificial intelligence-based networks were developed that utilize sensor-based feedback on a mechanized GTAW head. We present an image-based semantic segmentation convolutional neural network that identifies crucial features such as the weld pool, groove, wire, and electrode based on which geometric measurements are derived. A separate novel neural network predicts the weld bead geometry for multi-pass welds and inconsistent groove geometries. The application of both neural networks is a pre-requisite that enables the autonomous planning and execution of multi-pass welds to fill a groove.

1 Introduction

In typical gas tungsten arc welding (GTAW) processes, a skilled welder is needed to constantly observe the welding process and make adjustments when they observe any disturbances to ensure a good weld that is free of defects. In GTAW, the wire is fed externally into the arc. There exists an optimal wire position in the molten pool such that no defects are introduced as a result of poor wire placement. Examples of other criteria that can introduce weld defects are, the change in the wire cast, arc gap, deposition rate, and/or the prior weld bead can all change the location of the wire. Thus, a welder must constantly observe if the wire is out of place and make the necessary corrections to account for these possibilities. The welding parameters are also crucial for the welding process. The electrode position inside the groove, the power induced by current, and the wire deposition rate induced by the travel and wire feed speed all have a direct impact on the bead geometry. Skilled welders can estimate the weld bead geometry based on the input welding parameters, but the everchanging multi-pass profile groove makes this a challenge for even the most experienced of welders.

Humans observing and predicting the weld in real time takes great skill, and that same group of skilled welders are expected to retire from the work force [1]. The demand for skilled welders is high, but the current incoming welders will not be enough to fill the gap in the market. Therefore, there is a need to automate the manual human interaction during the welding process. Such that a program can use sensor feedback to replicate the complex decision making a skilled welder performs during a nuclear plant weld repair. Hence, artificial intelligence (AI) in the form of neural networks processing multimodal sensor data that can accomplish a fully adaptive feedback welding system is needed.

2 Related Work

Predicting the weld bead geometry has been a difficult challenge that is needed for adaptive welding to properly select welding parameters that result in a suitable weld bead geometry. Typically, the input parameters of a predictive model are the bead geometry influencing welding parameters and the cross-sectional shape of the existing groove. In this field, artificial neural networks in particular have proven to be suitable for this type of prediction [2, 3, 4]. Many approaches rely on approximations of the current weld groove by using key features such as width and height of the groove or weld bead of previous passes and approximate the resulting weld beads through, e.g., parabolas. However, this assumes that both the groove geometry and the weld bead can be sufficiently approximated by these geometric features, making it inherently less versatile and less accurate.

Apart from off-line weld bead prediction, it can be necessary to control the welding process in real-time. For this, different image-based methods using neural networks have only recently been tested. One approach first predicts the absolute pixel coordinates of certain objects of interest using a convolutional neural network (CNN) and then calculates e.g., the distance of the wire relative to the groove to further steer the process [5]. Directly regressing coordinates from an image is, however, a difficult task for plain CNNs due to their inherent lack of absolute spatial knowledge [6].

The authors of [7] propose a semantic segmentation approach to automatically segment important laser-welding regions such as the weld pool and weld seam,

*Corresponding authors: {stefan.mann@ilt.fraunhofer.de, jtatman@epri.com}

post-process their geometrical features and subsequently detect welding defects. Latest research in neural networks and computer vision in particular has allowed the technology to grow exponentially and in combination to ever increasing performance of graphics cards makes them a reasonable choice for in-situ process control. Therefore, a convolutional network similar to [7] is trained on GTAW processes to evaluate the capabilities of semantic segmentation networks [8] for in-situ steering of welding processes and a holistic multimodal bead prediction model is presented as a prerequisite for automated off-line parameter planning.

3 Technical Background

The basis for all experimental testing and development was done on a 6 axes track based mechanized GTAW weld head, Fig. 1. All axes were fully equipped with position encoder-based feedback to ensure the repeatability of the weld process. In addition to using Liburdi Dimetrics's V weld head [9], a Liburdi Goldtrack VII [10] was used as the main welding power supply. The weld head was modified to support 3 sensors. A Cavitar C300 welding camera [11] utilizes laser illumination to completely filter the arc light from images. This camera, mounted on the leading edge of the weld head, monitors the wire entering the weld pool. A Keyence LJ-V7080 laser profilometer [12] that generates a 2-D profile of the surface topology. This profilometer monitors the weld bead solidification in real time and after welding concludes. A Xarion Eta250 Ultra [13] laser microphone capable of sensing frequencies between 10 Hz – 1 MHz.

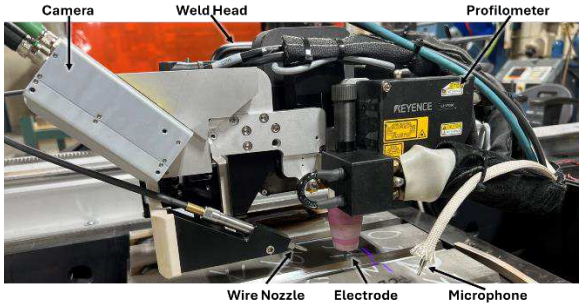

Fig. 1. GTAW Adaptive Welding System with Sensors.

To accomplish GTAW adaptive welding, there are two processes that must be controlled for which neural networks can be used. Real time closed loop control of the wire position in the weld pool. As well as a pre-processing open loop control of the welding parameters involved to adaptively fill a groove. Both processes require the foundation of neural networks to control the weld process. A network to identify features in the weld, and a network to predict the weld bead geometry.

To build the neural network, large experimental data sets were created for training. All sensors were controlled by a separate PC operating a LabVIEW program. During welds, LabVIEW triggers the acquisition of images, axes positions, profiles, and weld telemetry data from the sensors and saves them onto to the PC. All data acquisition were synchronously collected. All welds were made inside a machined trapezoidal groove. This groove type assumes that the root and hot passes were already complete, hence only requiring the fill and cap passes to be welded. At the start, there was a strict design of experiments (DOE) developed to initially evaluate the wire position how the welding parameters impact the weld bead, Table 1.

Table 1. Welding Parameters Limits during Trials

	Lower Limit	Ideal	Upper Limit
Electrode Position	-0.35 inch	N/A	0.35 inch
Current	120 Amps	200 Amps	350 Amps
Travel Speed	1 in/min	2.4 in/min	5 in/min
Wire Feed Speed	10 in/min	40 in/min	80 in/min

4 In-Line Processing

During a welding trial, multiple unforeseen external influences can negatively impair the welding process. Not only can these influences lead to uneven weld seams but can also lead to defects which cannot be repaired afterwards resulting in milling away the weld seam in the worst case or in case of not being detected in unsatisfactory deficient weld beads. As this is especially inacceptable in the field of welding for nuclear applications, in-line processing of sensor data is needed to assure a stable welding process.

4.1 Image-based Processing

In classical welding scenarios, an experienced welding operator is able react to uneven weld seams or even defective beads based on how the welding process looks like. Traditional image processing approaches have been shown to work well and reliably for a specific application, but once the image is out of normal configuration, the method fails [14]. To adapt these capabilities to welding robots and overcome constrained applications of classical Computer Vision algorithms, the Cavitar C300 welding cameras' images are processed by a CNN. More precisely, a semantic segmentation approach is chosen, as it allows to extract the most relevant parts of the welding process by automatically assigning each pixel to one of the objects in Fig. 2 enabling further downstream analysis of the segmented image.

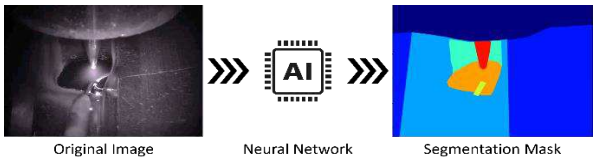

Fig. 2. Exemplary semantic segmentation of a TIG welding image.

A typical choice for semantic segmentation is a U-Net [15] which has been successfully applied to the segmentation of welding images [16]. However, over the past years, many improvements over the original U-shaped model architecture have been made resulting in both better performing and less computationally demanding neural network architectures. One of them is the DDR-Net [17] which includes a mechanism for the simultaneous processing of the image on different resolutions and intertwining the extracted knowledge of both lower and higher resolutions multiple times during the image processing. This helps to better identify both the borders of rather fine-granular objects like the tip of the wire while it is able to set it into the greater context using the internal lower resolution processing path.

To ensure the real-time capabilities of our approach, a DDR-Net-23-Slim was used since it demonstrated great results across multiple semantic segmentation datasets (i.e., Cityscapes) while maintaining inference speeds of >200Hz on consumer-grade hardware without prior down-scaling of the image. Since the welding camera outputs a grayscale image with a resolution of 1440 x 1080 pixels, the input shape of the neural networks is configured to the shape (1,1440,1080), allowing for full resolution segmentation masks.

Additionally, to ensure the real-time capability of the neural network and to reduce the computational overhead, the DDRNet-23-Slim [17] is used since it demonstrated great results across multiple semantic segmentation datasets (i.e., Cityscapes) while maintaining inference speeds of >200Hz on consumer-grade hardware without prior down-scaling of the image. Since the welding camera outputs a grayscale image with a resolution of 1440 x 1080 pixels, the input shape of the neural networks is configured to the shape (1,1440,1080), allowing for full resolution segmentation masks.

For training of the DDRNet-23-Slim, 250 random images of 20 different welding trials each and 250 random training of another 3 welding trials each have been manually labelled for training and validation, respectively. To make the neural network as robust as possible to different welding and setup scenarios (i.e., spatter, arc reflections, changes of illumination / camera angle) we employ several augmentation strategies on the mask and images such as randomly rotating the image, jittering the colour, and applying gaussian blur. Further, to cope for the imbalanced size of the different regions, a weighted CrossEntropy loss function is used and to track the training progress and prevent overfitting, the training is stopped once the validation data are showing continued non-improving Intersection over Union (IoU) metrics. As depicted in Fig. 3, from the output of the trained network, numerous measurements can be derived at once on a pixel scale based on the individual application.

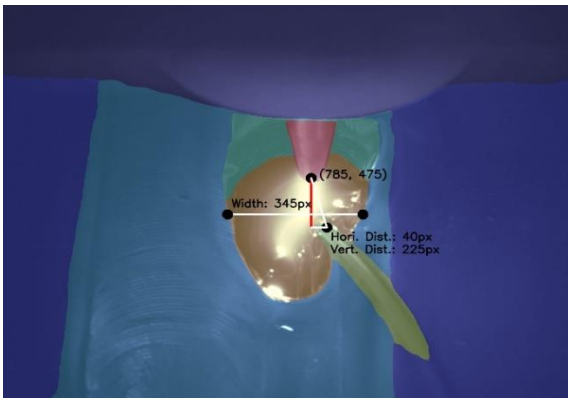

Fig. 3. Geometric analysis of a segmented TIG welding image. The visualized prediction is overlaid on the original image in color.

Exemplary use-cases could be the tracking of the weld pool's width, the position of the weld pool or the weld seam, the boundary of solidification of the weld pool or the position of the filler wire in relation to the electrode. Since the speed of the neural network is capable of processing many successive images per second, this approach allows not only the documentation of the welding process in single images, but also the tracking of different objects for a wide range of applications, as well as the correlation of different object positions over time, based on which different control strategies can be applied. This, however, presumes the robustness of the neural network to correctly detect the objects in different settings. Thus, we evaluate the network's capabilities in Section 6.1.

5 Off-Line Planning

In contrast to the unforeseen and unpredictable in-situ disturbances, there are certain geometrical properties that can be predicted to a certain degree. In the following, we propose a novel neural network architecture for predicting the resulting weld geometry based on the welding parameters and electrode position.

5.1 Bead Prediction

5.1.1 Neural Network Architecture

The resulting groove geometry of a GTAW process is mainly, but not exclusively dependent on a) the weld settings: arc voltage and current, travel speed and wire feed speed, b) the positioning of the electrode and c) the present groove geometry [18]. Additionally, there are many other weld settings such as the arc pulse duration, wire position, weaving of the electrode and different base materials that additionally influence the welding geometry. However, to not overly increase the parameter space, these parameters were kept constant throughout all welds and thus neglected by the neural network.

To use the profilometer and welding parameter data for predicting the resulting weld bead shape using a neural network, it is necessary to properly (pre-)process

and jointly correlate them. Since only the local area of the weld groove geometry influences the geometric outcome of the weld bead it is unnecessary to process the whole three-dimensional scanned groove. Thus, we follow related approaches [2, 3] and rely on using single, local two-dimensional scans of the groove. As during the welding trials the weld seams did not exceed 0.45 inches to the right and left of the tip of the electrode, we process input b) and c) by uniformly sampling 31 points of the two-dimensional scan in a range of 0.9 inches around the electrode tip's position. (Fig. 4, lower left)

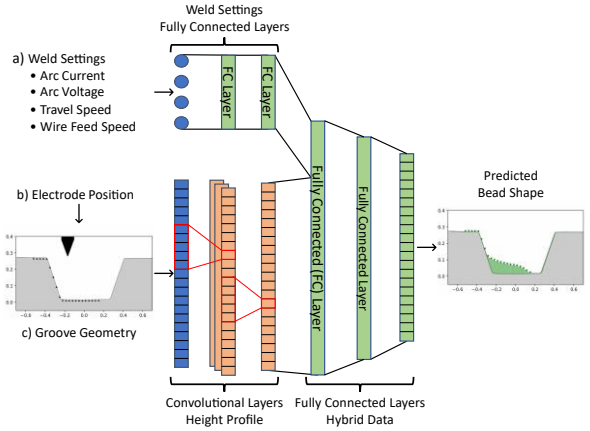

Fig. 4. Overview of the neural network architecture designed for bead prediction.

In contrast to the weld settings (Fig. 4, input a), these scans contain coherent height information and thus should be separately pre-processed before jointly processed with the weld settings. For that reason, residual, one-dimensional convolutional layers are applied to the sampled groove scan to extract local groove information, i.e., gradients or bumps in the current weld groove.

The numerical values of the weld settings already have a meaning on their own but are classically considered in combination when selecting the welding parameters, as they determine physical properties such as the effective heat input [19] and therefore are pre-processed with few fully connected layers on their own as well (Fig. 4, upper left).

After separately processing all inputs, they are combined via a multi-layer perceptron (MLP) block ending with a linear layer with 31 outputs on which the multinomial logistic regression function Softmax is applied to obtain a probabilistic density distribution. Here, each of the 31 outputs specifies what fraction of the theoretical cross-sectional area of the input filler volume is built up on that point. Thus, to obtain the actual predicted post-weld geometry, it is necessary to multiply the predicted relative distribution by the theoretical filler input A_{filler} in Eqn. 1, and add it onto the current pre-weld groove geometry:

$$A_{filler} = \frac{Travel\ Speed * A_w}{Wire\ Feed\ Speed} \quad (1)$$

$$G^{post} = \begin{pmatrix} G_1^{pre} \\ \dots \\ G_{31}^{pre} \end{pmatrix} + \begin{pmatrix} f_\theta(x_{params}, G^{pre})_1 \\ \dots \\ f_\theta(x_{params}, G^{pre})_{31} \end{pmatrix} * A_{filler} \quad (2)$$

where A_w denotes the cross-sectional wire area, G_i^{pre} the i-th sampled point of the pre-weld geometry and $f_\theta(x_{params}, G^{pre})_i$ the prediction of the neural network f based on its trained weights θ corresponding to the i-th sampled groove point.

Since the entire architecture is very shallow, an inference rate of more than 2 kHz can be achieved without further optimization making it feasible to quickly test multiple parameter settings.

5.1.2 Training

For training of the neural network, the pre- and post-weld scans of the Keyence Profilometer are required as well as the set welding parameters. As aforementioned, 31 points of the pre-scan weld geometry are uniformly sampled in a range of 0.9 inches. However, since the neural network predicts a relative bead distribution, the post-weld scans cannot be directly used as the training target but are first required to be converted into relative weld bead distributions (Fig. 5, red) by subtracting the post and pre-scans and are sampled afterwards respectively. The final step of pre-processing is a min-max normalization of both the groove geometry and weld settings.

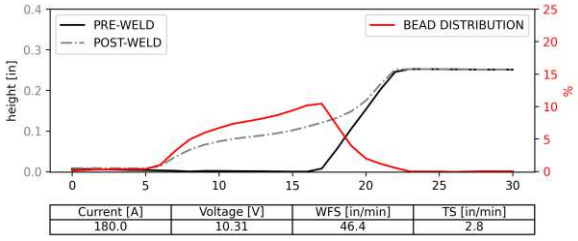

Fig. 5. Visualized training sample for the neural network.

In total, data of 30 (partially multi-) pass trials, translated to 83 welding passes were collected resulting in about 230,000 individual height profiles. To create a robust prediction, a dataset was built upon weld pass profiles from different stages of filling a groove and we deliberately selected many different welding parameter options. The extents of which are shown in Table 1 and saved the scans together with the height profiles. Similarly, to the training of the image-based neural network, the data is split into training and validation welding passes to monitor the training progress, prevent overfitting, and ensure a fair evaluation.

Since the network is designed to predict a density distribution, the Kullback-Leibler divergence [20] loss is used as the loss function where the original final Softmax function is replaced by a LogSoftmax function during training. In addition, we chose to randomly rotate the height profile very slightly, randomly apply minor left-right jitter to the position of the electrode and randomly flip the height profile horizontally as augmentation strategies to prevent early overfitting and artificially increase the different, individual training samples. The proposed neural network for bead prediction is evaluated in Section 6.2.

6 Results

6.1 Semantic Segmentation Network

For evaluation of semantic segmentation networks, typically the IoU, also called Jaccard Index, is used. It is based on the ratio of the overlap between the predicted and the labelled area and the union over both predicted and labelled area.

The final class-specific evaluation metrics of the neural network itself are shown in Fig. 6. In the violin plot, the deviation of the class specific IoU values of all testing images are depicted. To ensure robust real-time control during inference of the network, it is particularly important that a high IoU is achieved throughout the whole welding trial. The mean IoU values for the Weld Seam, Weld Pool, Filler Wire and Electrode are 0.792, 0.784, 0.936 and 0.872, respectively.

Note that because the labels were manually created using polygons in LabelMe [21], rounded objects such as the weld pool are difficult and time-consuming to map, and difficult to distinguish due to difficult lighting conditions, making a validation IoU of 1 very unlikely for these objects. Also, for relatively small objects like the Filler Wire or Electrode, slight mislabelled or falsely predicted areas have a greater impact to the IoU, explaining the outliers compared to the less dynamic classes.

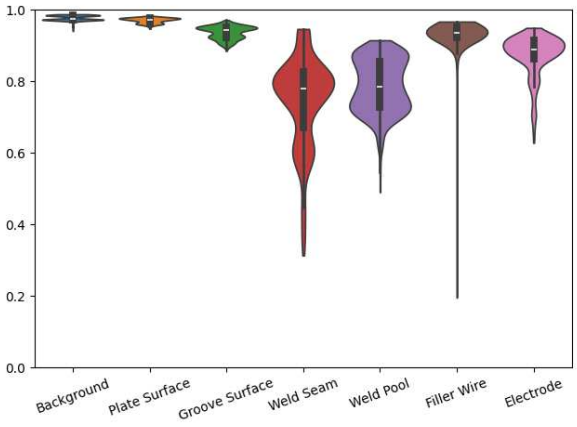

Fig. 6. Violin plots of IoU metrics over all TIG welding test-set images.

Furthermore, since the neural network only processes single images, it cannot obtain temporal contextual information to process locally poorly illuminated or obscured regions more robustly, such as the solidification boundary of the weld pool. Even for humans during the annotation process, the boundaries of certain objects are not always clear and thus required the contextual information of previous images.

Based on the geometrical analysis of the image, the objects of interest can be tracked over time. As a qualitative example, we calculated the horizontal offset between the (predicted) tip of the wire and the electrode which is shown in Fig. 7. Here, although the network was trained on images of groove welds, the underlying welding trial was not carried out in a weld groove but on a flat plate instead to assess the generalizability of the network. Despite the different welding scenario, the network exhibits accurate predictions resulting in no outliers of the raw geometrical measurements during the whole welding trial (1800 frames) and even showing minor wire oscillations introduced by the weld pool dynamics. Since these values could be used directly for further control of the welding robot, they illustrate the capabilities of semantic segmentation-based adaptive real-time process control.

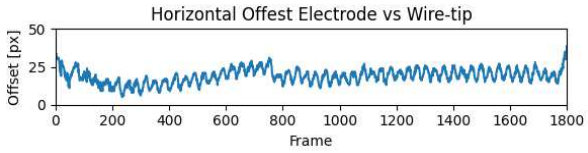

Fig. 7. Raw geometrical measurements from segmented image. No filtering applied.

6.2 Bead Prediction Network

For validation of the bead prediction using the proposed neural network architecture, not only different welding trials representing the different welding parameters (Table 1) were selected, but also later fill and cap passes from different multi-passes to assess various pre-weld groove geometries. Further, to investigate the needed complexity and concrete structure of the network, three different sizes are compared. Each size follows the general architectural proposal but varies in e.g., number of layers and filters of the convolutional layers, number of artificial neurons in the MLP block, etc.

Here, in Table 2, we present both the raw prediction performance by evaluating the density prediction using the Wasserstein distance, also called Earth Mover Distance (EMD), and the applied prediction after multiplying the relative distribution by the cross-sectional area A_{filler} and adding it to the pre-weld scan in Eqn. 2. For this, the IoU is used to report the intersecting area between predicted and actual bead area divided by union of predicted and actual area. Intuitively, the EMD of the bead prediction states the relative proportion that needs to be shifted by 0.1 inch proportionally to retrieve the actual bead distribution. That is, a EMD of 0.12 indicates that on average, 12% of the prediction is off by 0.1 inches, or 6% is off by 0.2 inches, etc.

Table 2. Evaluation of different Bead Prediction Model sizes.

	Small Model	**Medium Model**	**Large Model**
IoU	0.7739	0.8487	0.8504
EMD	0.3297	0.1702	0.1849
Inference Rate [Hz]	~2,900	~2,500	~2,400
#Parameters	~5,750	~7,250	~14,830

Due to the small number of parameters, all neural networks achieve inference rates of >2kHz running on a 12th generation intel i7 processor, making further, potentially extensive use-cases of the neural network possible.

7 Discussion & Outlook

In this paper, we have shown two distinct approaches for the development of an autonomous adaptive welding robot. On the one hand, a semantic segmentation based neural network illustrated its capabilities to detect different TIG-welding specific objects accurately and robustly in various welding scenarios based on which geometrical features can be calculated. It has been shown that these features are useful for the documentation of the welding process but because of the fast inference times of the underlying segmentation network also enable further image-based in-situ process control for a broad range of applications. This allows welding robots to partially understand the complex observations of human welding operators and subsequently to automatically correct themselves and therefore ensure even weld seams and prevent qualitative defects during the weld passes. These scenarios need to be examined closer in future work. The Cavitar C300 is a widely adopted welding camera in industry. While it is worth evaluating different cameras as well as more context-aware video segmentation, we focused on image segmentation as the needed hardware for it is way more accessible. However, it could be beneficial to use cameras with more than one grayscale channel to enhance the segmentation performance on single images and investigate the performance versus inference time trade-off through contextual video segmentation. Current work has shown success when applying the model towards R.G.B. channels.

On the other hand, a novel approach for geometrical bead prediction is presented. The proposed neural network overcomes the inherent limitations induced through (mostly parabolic) approximations of other bead prediction approaches by directly using the absolute cross-sectional height information of the scanned groove. Also, instead of relying on mathematical parabolic approximations of the resulting bead shape, a density distribution is predicted to determine the percentage of accumulated filler material at different points of the cross-sectional groove. The evaluation of the proposed neural network shows promising results. In combination with the high inference rate of >2kHz without specialized hardware, the model could enable the automated search for the geometric-wise optimal set of welding parameters. The general methodology for this, however, needs to be investigated. Also, as the neural network only considers the Arc current and voltage, wire feed speed and travel speed, larger neural networks with more inputs could be used to properly represent different welding scenarios.

8 Declarations

8.1 Conflict of Interest

The authors declare no competing or conflicts interests.

8.2 Funding

Electric Power Research Institute (EPRI) had internally funded all research, equipment, and contracts for pursuing work on this project. EPRI receives a majority of its funding from memberships who work in the energy sector as well as government sectors across the world. This funding is then redistributed amongst multiple groups to pursue research for the energy sector whether that be in nuclear, power grid, fossil fuels, etc. The current study, as discussed in this paper, was a part of the internal EPRI research project for the Nuclear Plant Support “Adaptive Feedback Welding” which is currently managed by the Welding Research and Technology Center (WRTC) at EPRI. The focus of this project was to develop a method for automating the GTAW welding process and adaptively make changes to account for changes during the process. Fraunhofer ILT is a group that EPRI contracted to assist in the development of artificial intelligence-based algorithms as described in this paper. EPRI is a non-profit organization and has no interest in making a profit from this project.

9 References

[1] American Welding Society, “Shining a light on the welding workforce.,” AWS, 2024. [Online]. Available: https://weldingworkforcedata.com/. [Accessed 12 May 2024].

[2] C. M. Horváth, J. Botzheim, T. Thomessen and P. Korondi, “Bead geometry modeling on uneven base metal surface by fuzzy systems for multi-pass welding,” *Expert Systems with Applications,* vol. 186, 2021.

[3] S. Yan, S. Ong and A. Nee, “Optimal Pass Planning for Robotic Welding of Large-dimension Joints with Deep Grooves,” *Procedia CIRP,* vol. 56, pp. 188-192, 2016.

[4] S. Juang, Y. Tarng and H. Lii, “A comparison between the back-propagation and counter-propagation networks in the modeling of the TIG welding process,” *Journal of Materials Processing Technology,* vol. 75, pp. 54-62, 1998.

[5] J. Bialach, M. Wright and R. Pistor, “Adaptive Welding”. Canada Patent WO/2024/089469, 23 October 2023.

[6] R. Liu, J. Lehman, P. Molino, F. Petroski Such, E. Frank, A. Sergeev and J. Yosinski, “An intriguing failing of convolutional neural

networks and the CoordConv solution," *NeurIPS,* vol. 31, 2018.

[7] C. Knaak, G. Kolter, F. Schulze, M. Kröger and P. Abels, "Deep learning-based semantic segmentation for in-process monitoring in laser welding applications," in *Applications of Machine Learning*, San Diego, 2019.

[8] J. Long and E. Shelhamer, "Fully Convolutional Networks for Semantic Segmentation," Berkeley, 2015.

[9] Liburdi Automation Inc, "V HEAD," Liburdi Dimetrics, July 2023. [Online]. Available: https://www.liburdidimetrics.com/weldheads/v-head. [Accessed 2024].

[10] Liburdi Dimetrics, "GOLD TRACK VII," Liburdi Dimetrics, November 2023. [Online]. Available: https://www.liburdidimetrics.com/powersupplies/gold-track-vii. [Accessed 2024].

[11] CAVITAR LTD, "Cavitar Welding Camera," 2024. [Online]. Available: https://www.cavitar.com/product/cavitar-welding-camera/. [Accessed 2024].

[12] Keyence Corporation of America, "High-speed 2D Laser Profiler," Keyence, 2024. [Online]. Available: https://www.keyence.com/products/measure/laser-2d/lj-v/models/lj-v7080/. [Accessed 2024].

[13] XARION Laser Acoustics GmbH, "Eta250 Ultra Optical Microphone," 2024. [Online]. Available: https://xarion.com/en/products/eta250-ultra. [Accessed 2024].

[14] S.-E. Belhout, "Image Based Processing for Weld Defect Detection," Tennessee Research and Creative Exchange, Knoxville, 2022.

[15] O. Ronneberger, P. Fischer and T. Brox, "U-Net: Convolutional Networks for Biomedical Image Segmentation," *International Conference on Medical Image Computing and Computer-Assisted Intervention,* p. 234–241, November 2015.

[16] R. Yu, J. Kershaw, P. Wang and Y. Zhang, "Real-time recognition of arc weld pool using image segmentation network," *Journal of Manufacturing Processes,* vol. 72, pp. 159-167, December 2021.

[17] Y. Hong, H. Pan, W. Sun and Y. Jia, "Deep Dual-resolution Networks for Real-time and Accurate Semantic Segmentation of Road Scenes," *IEEE Transactions on Intelligent Transportation Systems,* 2022.

[18] A. D. Sarolkar and D. K. P. Kolhe, "EFFECT OF PROCESS PARAMETERS ON WELD BEAD GEOMETRY AND MICRO-HARDNESS OF WELDING AA 6082 USING GTAW PROCESS," *Journal of Emerging Technologies and Innovative Research (JETIR),* vol. 4, no. 10, October 2017.

[19] J. K. Tatman, "Development of Improved Equations for Weld Heat Input and Dilution Control," ASME 2018 Pressure Vessels and Piping Conference, Prague, Czech Republic, 2018.

[20] S. Kullback and R. A. Leibler, "On information and sufficiency," *The annals of mathematical statistics,* vol. 22, no. 1, pp. 79-86, 1951.

[21] B. C. Russell, A. Torralba, K. P. Murphy and W. T. Freeman, "LabelMe: a database and web-based tool for image annotation," *INTERNATIONAL JOURNAL OF COMPUTER VISION,* vol. 77, no. 1-3, pp. 157-173, May 2008.